Shock Loading of IFE Reactor Cooling Tubes

**M.H. Anderson, J.G. Oakley, M.A. Coil,
R. Bonazza, R.R. Peterson**

October 2000

UWFDM-1145

FUSION TECHNOLOGY INSTITUTE

UNIVERSITY OF WISCONSIN

MADISON WISCONSIN

SHOCK LOADING OF IFE REACTOR COOLING TUBES

M. H. Anderson, J. G. Oakley, M. A. Coil, R. Bonazza and R. R. Peterson
University of Wisconsin - Madison
1500 Engineering Dr., Madison, Wisconsin, 53706
Phone: 608-263-2802 Fax: 608-263-4499
email: manderson@engr.wisc.edu

ABSTRACT

Many inertial confinement fusion (ICF) reactor designs incorporate a bank of cooling tubes as the first structural wall. These tubes provide important functions such as heat transfer and fuel breeding and must endure the cyclic impact of the shock waves formed from reaction of the fuel. Shock tube experiments and parallel numerical studies are conducted for shock waves incident on banks of instrumented cylinders meant to simulate the first wall of cooling tubes. Images of diffracted shocks, cylinder surface pressure traces, and calculated force distributions describe the interaction between the shock and the bank of cylinders. The numerical model shows good agreement with the experimental data.

I. INTRODUCTION

In proposed inertial confinement fusion (ICF) reactors, an array of cooling tubes comprises the first structural wall. Proposed schemes include the Inhibited Flow in Porous Tubes (INPORT) and Perforated Rigid Tube (PERIT) designs[1]. Both designs consist of hollow tubes carrying a PbLi eutectic alloy. The INPORT tubes are made of a porous orthogonal weave of SiC, C, or steel that allows an ablative film of the PbLi to form on the outer surface of the tube. This film absorbs x-rays and target debris. The bulk of the liquid flowing through the tube absorbs the photon and neutron energy and mitigates the isochoric heating by the neutrons. The first few levels of the PERIT design have fan sprays that create a liquid sheet of PbLi. This liquid sheet serves the same purpose as the protective liquid film in the INPORT design. These tubes must be able to withstand the impact of the shock wave formed by the thermonuclear reaction of the deuterium-tritium (DT) fuel. Adequately designing the protection for the first wall requires understanding the impulsive shock loading on the tubes. The impulsive loading on the tubes can be understood by studying the interaction of a transient shock wave incident on a cylinder or bank of cylinders. Previous studies include analytical investigations of the shock-refraction phenomenon,[2,3] numerical simulations of the flow around a cylinder,[4,5,6] and experimental flow visualizations and pressure measurements[7,8,9,10]. These studies provide detailed knowledge of the fluid dynamics around a single cylinder. However, the existing literature contains little work specific to the geometries relevant to the ICF designs.

In an attempt to understand the loading on the first wall of proposed ICF reactors, this work employs a shock tube to study the interaction of incident shocks on a bank of cylinders. Parallel experiments and numerical modeling examine the shock pattern formation and the resulting pressure loads on the cylinders.

II. EXPERIMENTAL DESCRIPTION

Figure 1 shows the shock tube used in the experiments. The vertical shock tube is 9.2 m long and is designed to withstand a 20 MPa pressure load. Using helium as the driver gas and argon as the driven gas, the tube can achieve strong shocks, up to Mach 5, in gas at STP. Measuring the time between pulses at two pressure transducers mounted in the driven section quantifies the shock speed. The driven section has a large square inner cross section measuring 25.4 cm x 25.4 cm. The parallel walls enable good flow visualization in the test section. Two 22.0 cm diameter fused

silica windows on opposing walls allow optical access to the test section. Anderson et al. provide a detailed description of the shock tube[11].
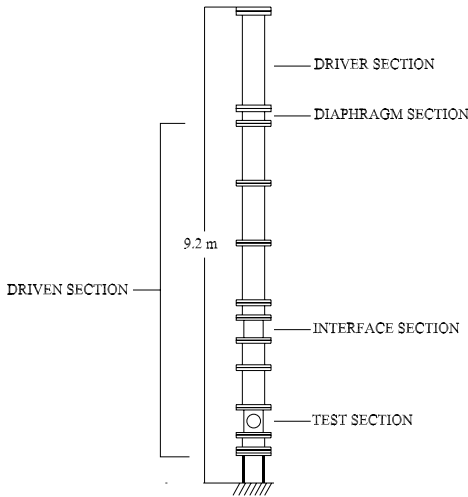

Figure 1: Schematic of Wisconsin shock tube.

Figure 2 shows the bank of three cylinders that mounts in the test section. The size and spacing of these cylinders represent the geometry of the cooling tube arrangement in an ICF reactor. The two small cylinders, positioned to see the shock wave first, measure 0.0538 m in diameter. The single, larger center cylinder sits 0.0592 m below the centers of the smaller cylinders and measures 0.0635 m in diameter. The cylinders are aligned perpendicular to the windows and the ends are flush with the window surface.
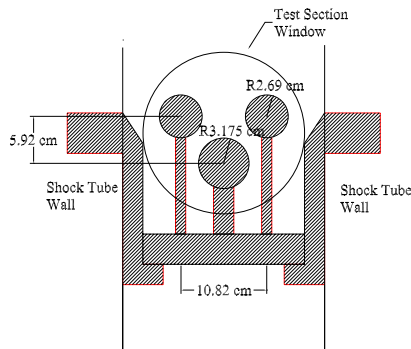

Figure 2: Side view of bank of cylinders detailing tube size and aspect ratio.

Eight pressure transducers (PCB, model 112A03) acquire the surface pressures on the large and one of the small cylinders. As Figure 3 shows, the transducers are mounted at 30° increments. Rotating the cylinders

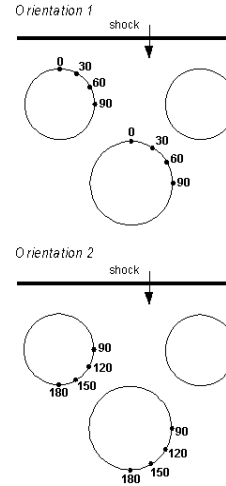Figure 3: Cylinder arangements instrumented with pressure transducers.

by 90°, from orientation 1 to orientation 2, provides pressure measurements from 0° to 180° with respect to the top of the cylinder. An HP Infinium oscilloscope acquires the four pressures from the smaller cylinder; a National Instruments data acquisition board (PCI-6110: 12-bit, simultaneous sampling multifunction I/O board) acquires the four pressures from the larger cylinder. All pressure measurements are sampled at 1 MHz. Five experiments are conducted for each of the orientations shown in Figure 3. Conducting multiple experiments provides a visual time series of the shock passing over the cylinders. The pressure traces for each location on each cylinder are averaged together for comparing results with the numerical model calculations.

Figure 4 shows the setup used to acquire an image from each run. The light source is one head of a Continuum Surelite II-PIV pulsed Nd:YAG laser. The pulse is 10 ns in duration and can deliver up to 220 mJ/pulse at a wavelength of 532 nm. A series of mirrors directs the beam to the appropriate path. Two lenses overexpand the beam, allowing the central, most uniform section of the beam to fill the first mirror. A 0.3 m circle of collimated light reflects off the second mirror and illuminates the windows in the test section. The image is visible on a screen placed outside the window of the test section. A Pixel Vision CCD camera (back-lit 1024 x 1024 pixel array) focused on this screen captures the image. A specified time delay from the shock passing a pressure transducer above the test section synchronizes the laser pulse with the desired position of the shock. Each experiment captures one image.
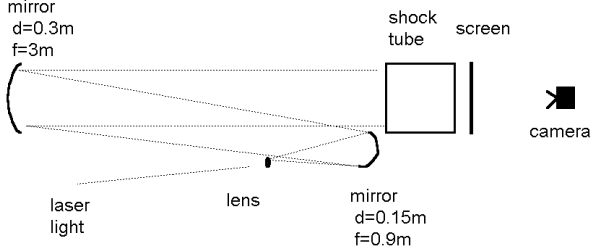
2

Figure 4: Shadowgraph setup.

III. MODELING

Numerical modeling simulates the experiments conducted in the shock tube. Because the experiment is quasi-two-dimensional, a two-dimensional (2D) model is employed. An exact Riemann solver solves the inviscid, time-dependent Euler equations. The code uses a Godunov integration method for updating the values to the next time step[12]. Numerical schlieren images are generated for comparison with the experimental shadowgraph images[14]. Equation 1 gives the equations in conservation form.

$$\mathbf{U}_t + \mathbf{F}(\mathbf{U})_x + \mathbf{G}(\mathbf{U})_y = 0 \qquad (1)$$

Equation 2 gives the conservation variables $\mathbf{U}$ and the fluxes $\mathbf{F}$ and $\mathbf{G}$.

$$\mathbf{U} = \begin{pmatrix} \rho \\ \rho u \\ \rho v \\ E \end{pmatrix}; \mathbf{F} = \begin{pmatrix} \rho u \\ \rho u^2 + p \\ \rho uv \\ u(E+p) \end{pmatrix}; \mathbf{G} = \begin{pmatrix} \rho v \\ \rho uv \\ \rho v^2 + p \\ v(E+p) \end{pmatrix} \qquad (2)$$

Equation 3 gives the total energy per unit volume.

$$E = \rho \left[\frac{1}{2}(u^2 + v^2) + e \right] \qquad (3)$$

Using the calorically ideal gas model, equation 4 provides closure.

$$e = \frac{p}{\rho(\gamma - 1)} \qquad (4)$$

A splitting scheme is employed for the two spatial dimensions. The x-sweep solves equation 5;

$$\begin{pmatrix} \rho \\ \rho u \\ E \\ \rho v \end{pmatrix}_t + \begin{pmatrix} \rho u \\ \rho u^2 + p \\ u(E+p) \\ \rho uv \end{pmatrix}_x = 0 \qquad (5)$$

and the y-sweep solves equation 6;

$$\begin{pmatrix} \rho \\ \rho v \\ E \\ \rho u \end{pmatrix}_t + \begin{pmatrix} \rho v \\ \rho v^2 + p \\ v(E+p) \\ \rho uv \end{pmatrix}_y = 0 \qquad (6)$$

The tangential velocity components, v (u) in the x-sweep (y-sweep), are passively advected with the normal velocity component, u (v). A two-step process, shown in equations 7 and 8, accomplishes the integration from time n to n+1.

$$\mathbf{U}_{i,j}^{n+1/2} = \mathbf{U}_{i,j}^n + \frac{\Delta t}{\Delta x}(\mathbf{F}_{i-1/2,j}^n - \mathbf{F}_{i+1/2,j}^n); \forall j \qquad (7)$$

$$\mathbf{U}_{i,j}^{n+1} = \mathbf{U}_{i,j}^{n+1/2} + \frac{\Delta t}{\Delta x}(\mathbf{G}_{i,j-1/2}^{n+1/2} - \mathbf{G}_{i,j+1/2}^{n+1/2}); \forall j \qquad (8)$$

An exact Riemann solver with a Newton-Raphson iterative solver solves for the primitive variables (density, pressure and velocity) at each cell interface. The cell interface variables are used to compute the flux terms at the cell interfaces. The spatial accuracy is first-order, and the solution is updated in time with a $xyyx$ sweep order. An adaptive timestep is used for integration based on the maximum wave velocity during time n.

Circles situated as shown in Figures 2 and 3 represent the cylinders in 2D. The solution field is slightly larger than the window in the shock tube; the width of the domain matches the width of the square shock tube test section. The domain is a 25.4 cm square with a spatial resolution of 0.25 mm. The spatial discretizations, Δx and Δy, are equal, and the Cartesian grid is 1018 x 1018.

The runs presented here simulate a M=2.75 shock in argon. One-dimensional gas dynamics calculations provide the initial conditions. The top 5 cm of the domain contains argon with the post-shock properties; the rest of the domain contains quiescent argon at a temperature of 300 K and pressure of 101.325 kPa. The initial conditions for the shocked argon are a pressure of 933.129 kPa, a density of 4.63692 kg/m^3, and a particle velocity of 577.207 m/s. The north and south boundaries have extrapolated boundary conditions; the east and west boundaries are reflective to model the shock tube walls. Placing reflective boundaries at the cylinder-surface locations models the cylinders. The computation requires approximately 24 CPU hours on a Pentium III, 500 MHz machine.

IV. RESULTS

The results presented here represent shock experiments run with helium driver gas, argon driven gas, and a 20 gauge steel diaphragm between the driver and driven sections; this combination gives an average Mach number of 2.74 with standard deviation of 0.06. Shadowgraph images present the shock patterns, pressure traces present the pressure loads on the cylinders, and

3

forces calculated from the pressure data give an estimate of the impact on the cylinders. Comparisons show the agreement between the experimental and modeling results.
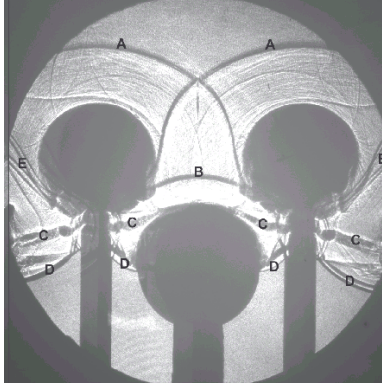

Figure 5: Shadowgraph image.

Figure 5 shows a shadowgraph image of the shock system captured 99 μs after the shock contacted the top of the upper cylinders. Letters mark the relevant features in the image. A's mark the shocks reflected from the smaller, upper cylinders. B marks the shock reflected from the larger, center cylinder. C's mark the contact discontinuities visible near the trailing edge of the smaller cylinders. D's mark the mach stems behind the smaller cylinders. E's mark features attributed to wall interactions.

Figure 6 compares shadowgraph images (left side) and the numerical results, which are presented in the form of schlieren images (right side)[14]. The experimental images were captured at times 36, 77, and 99 μs after the shock contacted the top of the upper cylinder. The numerical images show all of the key features visible in the shadowgraph images and indicate a good qualitative agreement between the 2-D code and the experimental results.

The force imparted on the cylinders gives an idea of the severity of the shock loading and allows a quantitative comparision to models. When the incident shock contacts the top of the cylinder and subsequently reflects, it imparts a large vertical dynamic load on the cylinder. The magnitude of this load varies with angle along the cylinder, because of the geometry of the shock system. The vertical impulse of a cylinder can be calculated from surface pressure measurements P(θ,t) using equation 9.

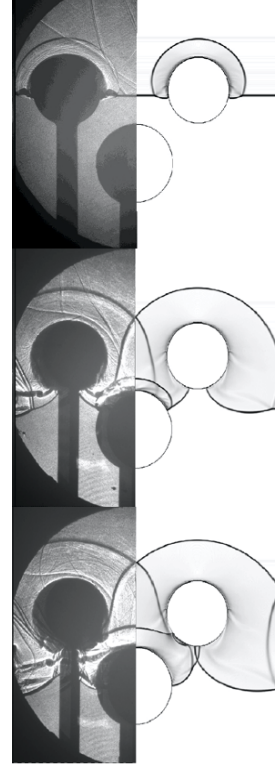$$I = \int_0^\tau 2 \int_0^{\theta_m(t)} P(\theta, t)^2 R cos^2(\theta) L d\theta dt; \qquad (9)$$

Figure 6: Comparison between experimental and numerical images (t=36 μs, t=77 μs and t=99 μs from initial contact with top cylinder), for a M=2.75 shock in argon.

Because the experimental pressure data is taken at discrete locations the vertical force as a function of time is approximated by Equation 10.

$$F_{vertical} = 2L[A_{0,15}(P_{0°} - P_{180°}) + \qquad (10)$$
$$A_{15,45}(P_{30°} - P_{150°}) +$$
$$A_{45,75}(P_{60°} - P_{120°})]$$

where
$$
\begin{aligned}
A_{0,15} &= R\left[\sin(15°) - \sin(0°)\right] \\
A_{15,45} &= R\left[\sin(45°) - \sin(15°)\right] \qquad (11) \\
A_{45,75} &= R\left[\sin(75°) - \sin(45°)\right],
\end{aligned}
$$

and the length of the cylinder, L, is 25.4 cm.

This equation multiplies the pressure at each angular location by the projected vertical area of the cylinder surface. Figure 7 shows force traces for the cylinders calculated from the numerical and the experimental results using Equation 10. As can be seen the maximum force is substantially higher on the lower cylinder due to an increase in shock strength as a result of the decreasing area as it passes through the first bank of tubes. The dip present in both the data and the numerical model

4

of the upper cylinder is a result of the reflection of the incident shock wave off of the lower cynder, which contacts the bottom of the upper cylinder, substantially decreasing the overall downward vertical force. This is consistent with the time sequence seen in Figure 7 where at appoximately 0.1 ms the reflection is seen to make contact with the upper cylinder. The slight increase in force on the lower cylinder at approximately 0.14 ms is the result of a second reflection of the wave off of the bottom of the upper cylinder making contact with the lower. The quantitative agreement between the numerical model and the data for both cylinders is quite good.
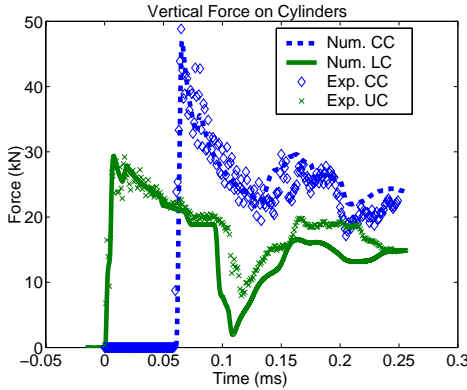

Figure 7: Force imparted on the cylinders: experimental and numerical data.

V. CONCLUSIONS

This work atempts to estimate the shock-induced loading on first wall cooling tubes in proposed ICF reactor designs. Shock tube experiments and accompanying numerical modeling efforts study the interaction between an incident shock wave and a bank of three cylinders intended to simulate the cooling tubes. The experiments image the shock formations and acquire surface pressures from the cylinders. Subsequent calculations from the pressure data yield the vertical force imparted on the cylinders. The model uses an Eulerian code to predict the results from the experiments. Comparisons between experimental and numerical images show good qualitative agreement in the reproduction of the features seen in the experiments. The force data over the cylinder also agrees well and gives a more quantitative comparison between the experiment and numerical model.

NOMENCLATURE

A	projected area
e	specific internal energy
i	grid point index in x-direction
j	grid point index in y-direction
L	length of cylinder
n	index on time
$F_{vertical}$	vertical force on cylinder
p	pressure
$P(\theta, t)$	pressure as a function of angle and time
P_θ	pressure from transducer at location θ
R	radius of cylinder
u	velocity in x-direction
v	velocity in y-direction
x	coordinate direction
y	coordinate direction
D_x	spatial time step in x-direction
D_y	spatial time step in y-direction
E	total energy per unit volume
F	flux in x-direction
G	flux in y-direction
U	conservation variable
ρ	density
γ	adiabatic exponent
θ	angle along cylinder
θ_m	angle subtended by shock

REFERENCES

1. Kulcinski, G.L., Peterson, R.R., and Moses, G.A., "Evolution of light ion driver fusion power plants leading to the LIBRA-SP design", *Fusion Technology*, v. **26**, pp. 849-856, 1994.

2. Bazhenova, T.V., Gvozdeva, L.G., Nettleton, M. A., "Unsteady interaction of shock waves", *Prog. Aerospace Sc.*, V. **21**, pp. 249-331, 1984.

3. Pavlov, V.A., "Diffraction of a strong shock wave on a cylinder with time varying radius", *J. App. Mech. Theor. Phys.*, v. **26**r n. 6, pp. 806-8, 1995.

4. Yang, J.Y., Liu, Y., and Lomax, H., "Computation of shock wave reflection by circular cylinders", *AIAA Journal*, v. **25**, n. 5, pp. 683-9, 1987.

5. Ofengeim, D.Kh. and Drikakis, D., "Simulation of blast wave propagation over a cylinder", *Shock Waves*, v. **7**, pp. 305-315, 1997.

6. Ofengeim, D.Kh., Syshchikova, M.P., Berezkina, M.K., and Sharov, D.M., "Some features of the

transient relaxation to a steady-state pressure on the surface of a cylinder acted on by a shock wave", *Tech. Phys. Lett.*, v. **19**, n. 7, pp. 471-3, 1993.

7. Bryson, A. E. and Gross, R.W.F., "Diffraction of strong shocks by cones, cylinders, and spheres", *J. Fluid Mech.*, v. **10**, n. 1, pp. 1-16, 1961.

8. Martin, V.C., Mead, K.F., and Uppard, J.E., "The drag on a circular cylinder in a shock wave", Atomic Weapons Research Establishment Report 0-34/67.

9. Bishop, V.J. and Rowe, R.D., "The interaction of a long duration shaped blast wave with an infinitely long right circular cylinder", Atomic Weapons Research Establishment Report 0-38/67.

10. Oakley, J.G., Puranik, B.P., Anderson, M.H., Peterson, R.R., Bonazza, R., Weaver, R.P., and Gittings, M.L., "An investigation of shock-cylinder interaction", London, ISSW22 paper 0171, 1999.

11. Anderson, M.H., Puranik, B.P., Oakley, J.G., Brooks, P.W., and Bonazza, R., "Shock tube investigation of hydrodynamic issues related to inertial confinement fusion", to appear in *Shock Waves*, Fall 2000.

12. Godunov, S.K., "A finite difference method for the computation of discontinuous solutions of the equations of fluid dynamics", *Mat. Sb.* 46, pp. 357-393, 1959.

13. Toro, E.F., Riemann Solvers and Numerical Methods for Fluid Dynamics, 2ed, Springer, 1999.

14. Quirk, J.J., "Amrita - A computation facility (for CFD modeling)", VKI 28th CFD Lecture Series, 23-27 February, 1998.